ChemComm

Teaching copolymerization catalysis to metal-organic frameworks by confining molecular catalysts in lattices

Journal:	*ChemComm*
Manuscript ID	CC-COM-01-2025-000500.R1
Article Type:	Communication

COMMUNICATION

Teaching copolymerization catalysis to metal-organic frameworks by confining molecular catalysts in lattices

Received 00th January 20xx,
Accepted 00th January 20xx

DOI: 10.1039/x0xx00000x

Chao-Yu Chiu,[a] Chia-Her Lin,[b] Pei-Wen Wu,[c] Zhuorigebatu Tegudeer,[d] Chen-Yen Tsai,*[c] and Wen-Yang Gao*[d]

Copolymerization catalysis remains underexplored compared to the broad range of other catalytic reactions promoted by metal-organic frameworks (MOFs). Here, we report a lattice-confinement strategy that immobilizes a highly active molecular complex within MOFs, transforming them into effective heterogeneous catalysts for copolymerization – that couples cyclohexene oxide and CO_2 into poly(cyclohexene carbonate) or integrate epoxide and phthalic anhydride into ester-ether copolymers. The encapsulated catalytically active species not only introduce new reaction patterns for MOFs but also enhance the structural robustness of the lattice, enabling the catalyst to be recycled multiple times.

Metal-organic frameworks (MOFs),[1-3] a class of crystalline porous materials, have been intensively investigated as heterogeneous catalysts for a variety of chemical organic transformations.[4-7] This has been driven by structural advantages of MOFs, including large accessible cavities to co-localize reagents, high degree of structural order for high-density active sites, controllable pore sizes to achieve fast mass diffusion or size/shape-dependent reaction selectivity, and functionalizable pore surface enabling task-specific design and multifunctionality.[8] Furthermore, the heterogeneous nature of MOF catalysts underpins the recyclability and ease of separation from products. The broad scope of transformations catalysed by MOFs ranges from Friedel-Crafts reactions,[9] condensation reactions,[10, 11] oxidations,[12-14] coupling reactions,[15] cyanosilylation,[16] carbon dioxide fixation reactions,[17-21] and many others.[22] Among them, MOF-enabled polymerization reactions remain relatively underresearched.[23]

Most known examples of MOF-enabled polymerization focus on alkene substrates,[24-28] with limited studies also exploring dienes,[29, 30] acrylamides,[31] methacrylates,[32-34] and cyclic esters.[35, 36] In these cases, catalytically active sites are derived either from unsaturated metal nodes or from postsynthetically functionalized centres that are often covalently linked to the framework. Here we describe a lattice-confinement strategy that encapsulates a highly reactive molecular complex into the cavities of MOFs,[37] achieving effective heterogeneous composite MOF catalysts for copolymerization reactions.[27, 38, 39] This heterogenization strategy immobilizes the active molecular complex as the guest species and still retains porosity for substrate access and product egress.

Another motivation behind this work is to develop a MOF catalyst that enables the coupling of epoxide and carbon

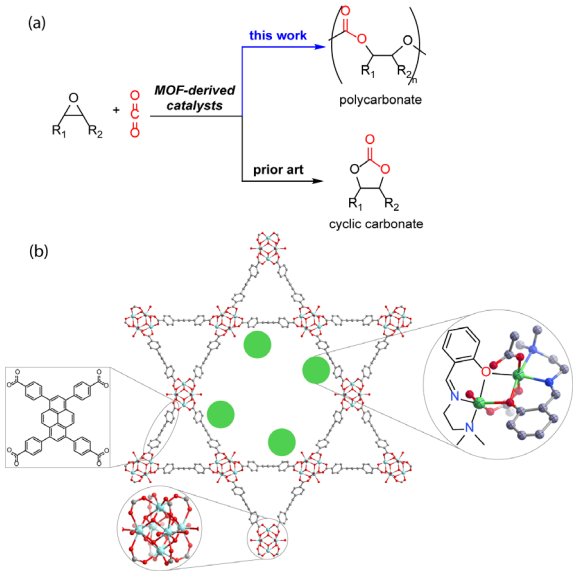

Figure 1. (a) This work highlights the first example of MOF-derived catalysts promoting the formation of polycarbonates between epoxides and CO_2, in contrast to cyclic carbonates as the product. (b) The active NNO-2Ni molecular complex (indicated by green dots) is confined in NU-1000 lattice to provide a MOF composite catalyst, which accomplishes copolymerization reactions that were not possible by NU-1000 itself.

[a] *Department of Chemistry, National Taiwan Normal University, Taipei 24449, Taiwan.*
[b] *Department of Chemistry, National Tsing Hua University, Hsinchu 300044, Taiwan.*
[c] *Department of Chemistry and Biochemistry, National Chung Cheng University, Chiayi 62102, Taiwan. E-mail: chyetsai@ccu.edu.tw*
[d] *Department of Chemistry and Biochemistry, and Nanoscale & Quantum Phenomena Institute, Ohio University, Athens, Ohio 45701, United States. E-mail: gaow@ohio.edu*

† Electronic Supplementary Information (ESI) available: Experimental details, PXRD patterns, infrared spectra, mass spectral data, SEM images, NMR spectra, pore size distribution plots and additional tables. For ESI see DOI: 10.1039/x0xx00000x

dioxide (CO_2) to produce polycarbonate directly, rather than cyclic carbonate, for the first time (Figure 1a). Although unsaturated metal centres within MOFs have been identified as Lewis acid sites and widely studied for CO_2 fixation with epoxides to form cyclic carbonates—transforming greenhouse gas into chemical feedstocks for value-added products[17-21]—no examples currently exist of MOF catalysts that facilitate the copolymerization of CO_2 and epoxide into polycarbonate.

Thus, to achieve the new form of polymerization based on MOFs, we envision that confining the active homogeneous catalyst species into ordered and porous MOF lattice remains highly promising. Inspired by our previous development of multinuclear nickel complexes for efficient copolymerization of CO_2 and cyclohexene oxide,[40] we initiated this work by postsynthetically encapsulating the selected dinuclear Ni complex (Figure 1b) into a known MOF, NU-1000,[41, 42] for characterizations followed by catalysis studies. NU-1000 was chosen due to its known thermal and chemical stability and hierarchical pores.

NU-1000 used in this work was synthesized by the solvothermal method and activated by HCl aqueous solution according to literature.[41, 43] NU-1000, being comprised of 8-connected hexanuclear $Zr_6(\mu_3\text{-}O)_4(\mu_3\text{-}OH)_4(H_2O)_4(OH)_4(COO)_8$ cluster nodes bridged by 1,3,6,8-tetrakis(*p*-benzoate)pyrene ligands (TBAPy, Figure 1b), represents a crystalline robust three-dimensional MOF featuring mesopores (>20 Å). Its obtained experimental powder X-ray diffraction (PXRD) patterns are consistent with the calculated ones (Figure S1). The shape of crystals observed in scanning electron microscopy image (Figure 2) also matches the one reported previously. N_2 adsorption isotherm at 77 K of the synthesized NU-1000 demonstrates an uptake capacity of 950 cm^3/g at P/P_0 = 0.9 (Figure S3), similar to the observed number in literature.[41] In addition, the pore size distribution derived from the N_2 adsorption isotherm exhibits three different pores with widths at 12.6 Å, 15.3 Å, and 33.8 Å (Figure S4), which match the reported values.[41] With confirmed NU-1000 in hand, we went ahead to immobilize the chosen complex of NNO-2Ni, $[L_2Ni_2(OAc)_2(OH_2)]$, which is a dinuclear Ni complex composed of two NNO-tridentate Schiff-base ligands (HL = 2-(((2-(dimethylamino)ethyl)imino)methyl)phenol), one monodentate acetate coordinating to one Ni(II) centre, the aqua ligand coordinating to the other Ni site along with the second acetate bridging two Ni(II) sites in a bidentate fashion. Each Ni(II) site gives an octahedral coordination geometry.

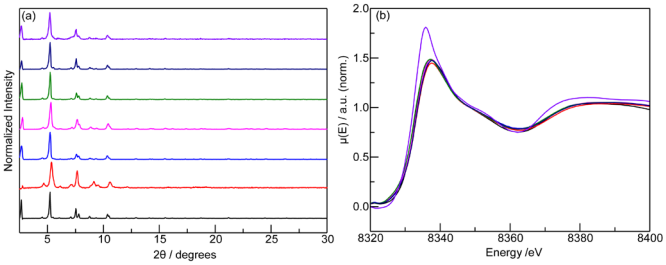

Figure 2. (a) PXRD patterns were collected on NU-1000 (—), NNO-2Ni-NU-1000 obtained by soaking NU-1000 in a range of NNO-2Ni EtOH solutions at different concentrations (NNO-2Ni(0.025)-NU-1000 (—), NNO-2Ni(0.050)-NU-1000 (—), NNO-2Ni(0.075)-NU-1000 (—), NNO-2Ni(0.100)-NU-1000 (—), NNO-2Ni(0.150)-NU-1000 (—), and NNO-2Ni(0.200)-NU-1000 (—)). (b) Ni K-edge X-ray absorption near edge spectra were presented for NNO-2Ni (—), $Ni(OAc)_2{\cdot}4H_2O$ (—), and the MOF composite samples (NNO-2Ni(0.025)-NU-1000 (—), NNO-2Ni(0.050)-NU-1000 (—), NNO-2Ni(0.075)-NU-1000 (—), NNO-2Ni(0.100)-NU-1000 (—), and NNO-2Ni(0.150)-NU-1000 (—).

The immobilization NNO-2Ni into NU-1000 was carried out by soaking NU-1000 (100 mg activated powder) into a series of ethanol (EtOH) solutions (5.0 mL) containing NNO-2Ni at a range of concentrations (0.025 M, 0.050 M, 0.075 M, 0.100 M, 0.150 M, and 0.200 M) at 80 °C for 24 h, respectively. The collected solids were washed by additional EtOH and dried at 80 °C under vacuum for further characterizations. The PXRD patterns of all the solids retain peak features of the parent NU-1000 (Figure 2a), illustrating the robustness of NU-1000 and structural integrity of the composite samples. N_2 adsorption isotherms at 77 K were also collected for respective composite samples (Figure S5). Overall, the encapsulated NNO-2Ni reduces the uptake amount of N_2 and fills up part of accessible pore space (Figure S6), compared to the parent NU-1000. Notably, the mesopore feature is well retained after the encapsulation, which enables the substrate diffusion.

Furthermore, the successful encapsulation experiments were evidenced by a suite of solid-state characterizations, including the X-ray photoelectron spectroscopy (XPS, Figure S7), X-ray absorption near edge spectroscopy (XANES, Figure 2b), and infrared spectroscopy (IR). For instance, the XPS spectra show an increasing trend for peaks corresponding to Ni 2p and N 1s signals upon changing the soaking solution concentration of NNO-2Ni from 0.050 M to 0.100 M. The Ni K-edge XANES spectra not only confirm the existence of Ni in all the composite materials, but also indicate +2 oxidation state for the Ni sites. The most straightforward proof from IR spectra (Figure S8) comes from the C–N stretching of amine derived from the NNO-2Ni complex being observed in the composite samples, given the complicated overlap of other vibrational signals.

Additionally, inductively coupled plasma optical emission spectroscopy (ICP-OES) was employed to quantify the amount of NNO-2Ni immobilized in NU-1000 upon digestion of the composite samples in acid. It was revealed that the NNO-2Ni(0.050)-NU-1000, obtained from the soaking solution at the initial concentration of 0.050 M, owns a formula of $(NNO\text{-}2Ni)_{0.54}@[Zr_6(\mu_3\text{-}O)_4(\mu_3\text{-}OH)_4(H_2O)_4(OH)_4(TBAPy)_2]$ and $(NNO\text{-}2Ni)_{0.43}@[Zr_6(\mu_3\text{-}O)_4(\mu_3\text{-}OH)_4(H_2O)_4(OH)_4(TBAPy)_2]$ for NNO-2Ni(0.100)-NU-1000 (See details in Table S1, electronic supplementary information, ESI). The relatively higher loading of NNO-2Ni in the NNO-2Ni(0.050)-NU-1000 sample than that of NNO-2Ni(0.100)-NU-1000 is further supported by the N_2 adsorption isotherms, which show a consistent lower N_2 uptake amount of NNO-2Ni(0.050)-NU-1000 than that of NNO-2Ni(0.100)-NU-1000 upon saturation.

Then we evaluated the reaction between CO_2 and cyclohexene oxide (CHO) with an aim to generate poly(cyclohexene carbonate) (PCHC) using the composite catalysts (NNO-2Ni-NU-1000, Tables 2 and 3). The control experiment was conducted using NU-1000 (50 mg) as the catalyst along with tetrabutylammonium bromide (TBAB, 0.10 mmol%) as the co-catalyst in the presence of CHO (35 mmol) and CO_2 initial pressure of 300 psi at 110 °C for 24 h, which delivered 37% conversion of CHO and *cis*-cyclohexene

Table 1. The reaction of CO_2 and cyclohexene oxide was attempted.

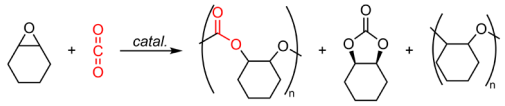

Entry	*Catal.*	*Co-catal.*	CHO conv. / %	CHC / % (*cis* only)	Polymer / % (PCHC / %)	Mn (*Đ*)
1	A	TBAB	37	>99	NA	NA
2	B	TBAB	94	75	25 (>99)	430 (1.17)
3	C	TBAB	68	94	6 (>99)	430 (1.17)
4	B	TBAC	87	66	34 (>99)	300 (1.17)
5	B	TBAI	65	77	23 (>99)	300 (1.17)
6	B	DMAP	65	83	17 (53)	660 (1.24)
7	B	9-AnOH	37	<1	>99 (<1)	8800 (1.78)
8	B	None	38	<1	>99 (<1)	8900 (1.91)

Reactions were carried out using 35 mmol cyclohexene oxide in the presence of NU-1000 (50 mg) or NNO-2Ni-NU-1000 (50 mg) as the catalyst and the choice of co-catalyst (0.10 mol%) under the initial CO_2 pressure of 300 psi for 24 h at 100 °C with a stir rate of 100 rpm. Catalyst A – NU-1000; Catalyst B – NNO-2Ni(0.050)-NU-1000; and Catalyst C – NNO-2Ni(0.100)-NU-1000. The conversion rates and the ratios of ester/ether were calculated based on ^{1}H NMR in $CDCl_3$:C_6D_6 (*v*/*v*=1:4.5) (details in ESI). The *trans*-CHC was not observed in any experiments. Mn(*Đ*) information was determined by GPC.

carbonate (*cis*-CHC) as the only product without any polycarbonate (Entry 1, Table 1). However, when NNO-2Ni(0.050)-NU-1000 (50 mg) was employed under the same reaction condition, 94% conversion of CHO was probed by NMR. Among them, 75% of CHO converted into *cis*-cyclohexene carbonate with 25% of CHO into PCHC (Entry 2, Table 1). Poorer catalytic performance was observed using NNO-2Ni(0.100)-NU-1000 (Entry 3, Table 1). The role of the co-catalyst—TBAB, tetrabutylammonium chloride (TBAC), tetrabutylammonium iodide (TBAI), or 4-dimethylaminopyridine (DMAP)—does not significantly affect the reaction, yielding both *cis*-CHC and PCHC as the products (Entries 4-6, Table 1). The observed PCHC polymer was verified by matrix-assisted laser desorption ionization–time of flight mass spectrometry (MALDI-TOF MS, Figure S9). Changing the co-catalyst from TBAB to 9-anthracenemethanol (9-AnOH) or removing the TBAB only produced polyether as the only product (Entries 7-8, Table 1).

To improve the selectivity of PCHC production, we investigated the role of the co-catalyst by increasing the amount of TBAB to 0.25 mmol% and 0.50 mmol% in the reaction. But the formation of PCHC was severely suppressed with *cis*-CHC as the only product (Entries 1-2, Table S2). Decreasing the reaction temperature from 110 °C to 80 °C using the catalyst of NNO-2Ni(0.050)-NU-1000 and TBAB (0.10 mmol%) for 24 h under the CO_2 initial pressure of 300 psi eventually resulted into PCHC as the only observable product (Entry 2, Table 2). Continuous attempts such as extending the reaction time to 48 h or increasing the CO_2 initial pressure to 500 psi did not lead to improved PCHC production (Entries 3-4, Table 2). Though the number average molecular weight of the PCHC remains to be further optimized, this still represents the first encouraging example of copolymerizing CO_2 and CHC to provide polycarbonate directly accomplished by MOFs. Moreover, the PXRD patterns collected on NU-1000 and its composites after catalysis trials indicate the encapsulated NNO-2Ni is beneficial to retain the crystallinity of the lattice, in contrast to NU-1000 becoming amorphous (Figure S10).

The second polymerization reaction we explored is the ring-opening copolymerization of epoxide with phthalic anhydride (PA)[39] promoted by the MOF composite. The expected polyesters, like the previously described aliphatic polycarbonates, are both viewed as environmentally benign alternatives and hold great promise for replacing non-biodegradable, petroleum-derived plastics. We tested NNO-2Ni(0.050)-NU-1000 (100 mg) for the reaction of CHO (35 mmol) and PA (35 mmol) in toluene (1.0 mL) along with the chain transfer agent of 9-AnOH (2.0 mol%) for 24 h at 110 °C in the beginning (Entry 1, Table 3). The result indicates both monomers exhibit relatively high conversion rates (>99% for CHO and 84% for PA), and the ester/ether ratio is identified as 30/70 in the product. Reducing the amount of 9-AnOH to half of its initial loading didn't improve the ester/ether ratio (Entry 2, Table 3). Conversely, increasing the loading of 9-AnOH to double or quadruple impacted on the ester/ether ratio, but also hindered the conversion of PA (Entries 3-4, Table 3). The formation of the copolymer was also confirmed by MALDI-TOF MS (Figure S11). Moreover, to demonstrate the advantage of heterogeneous MOF catalysts, we tested NNO-2Ni(0.050)-NU-1000 four more times (Table S3) after the initial catalysis and the last trial data were presented as Entry 5, Table 3. The results obtained along with PXRD (Figure S12) and the SEM image (Figure S13) demonstrate the MOF composite catalyst can be recycled without losing any activity.

To expand the scope of epoxide in the reaction, we tested propylene oxide (PO), 1,2-epoxy-4-vinylcyclohexane (VCHO),

Table 2. The reaction of CO_2 and cyclohexene oxide was catalysed by NNO-2Ni-1000 with TBAB as the co-catalyst.

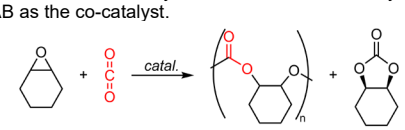

Entry	Temp. / °C	CO_2 pres. / psi	CHO conv. / %	CHC / % (*cis* only)	PCHC / %	Mn (*Đ*)
1	110	300	94	75	25	430 (1.17)
2	80	300	48	<1	>99	410 (1.12)
3	80*	300	68	96	4	420 (1.17)
4	80	500	83	>99	<1	NA

Reactions were carried out using 35 mmol cyclohexene oxide in the presence of NNO-2Ni(0.050)-NU-1000 (50 mg) as the catalyst and TBAB (0.10 mol%) as co-catalyst under the specified initial CO_2 pressure for 24 h at 110 or 80 °C with a stir rate of 100 rpm. No ether linkage polymers were observed in the reactions. The conversion rates and the ratios of ester/ether were calculated based on ^{1}H NMR in $CDCl_3$:C_6D_6 (v/v=1:4.5) (details in ESI). Mn(*Đ*) information was determined by GPC.*Entry 3 was kept for 48 h.

Table 3. The copolymerization reaction of cyclohexene oxide and phthalic anhydride was catalysed NNO-2Ni-NU-1000 with 9-AnOH as the chain transfer agent.

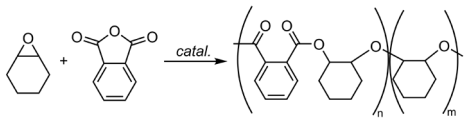

Entry	9-AnOH mol%	PA conv./%	CHO conv./%	Ester : Ether	Mn (*Đ*)
1	2	84	>99	30:70	1030 (1.31)
2	1	70	>99	30:70	1400 (1.30)
3	4	64	>99	60:40	800 (1.30)
4	8	58	>99	35:65	520 (1.25)
5	2	80	>99	30:70	2800 (1.37)

Reactions were carried out using 35 mmol CHO, 35 mmol PA in toluene (1.0 mL) in the presence of NNO-2Ni(0.050)-NU-1000 (100 mg) as the catalyst and 9-AnOH. The conversion rates and the ratios of ester/ether were calculated based on ^{1}H NMR in $CDCl_3$ (details in ESI). Mn(*Đ*) information was determined by GPC.

cyclopentene oxide (CPO) for the copolymerization with PA, respectively using NNO-2Ni(0.050)-NU-1000 (Table S4). The MOF composite proves to be a potent catalyst for these reactions, though future efforts will be devoted to improving the ester/ether ratio and the number average molecular weight of the product.

In conclusion, we leverage the lattice confinement strategy to introduce new MOF-based catalytic reaction patterns and successfully achieve catalyst recyclability. This work employs MOFs as solid hosts to support an active molecular complex within its pore space, thus combining the benefit of molecular precision and robust structural stability. By establishing a new avenue in MOF-based catalysis, we showcase the utility of these materials through two distinct copolymerization reactions: the conversion of cyclohexene oxide and CO_2 into poly(cyclohexene carbonate) and the integration of epoxide with phthalic anhydride to form ester-ether copolymers. While acknowledging the need for improvement in molecular weights of copolymers, we anticipate that this work will inspire further research into the development of MOF-based catalytic copolymerization systems.

The data supporting this article have been included as part of the Supplementary Information.

There are no conflicts to declare.

Acknowledgements

This research is supported financially by the National Science and Technology Council, Taiwan (NSTC 113-2113-M-194-011 to C.-Y. Tsai and NSTC 113-2113-M-003-015-MY2 to C.-H. Lin). W.-Y. Gao acknowledges partial support from the National Science Foundation under Grant No. [2345469].

References

1 H.-C. Zhou and S. Kitagawa, *Chem. Soc. Rev.*, 2014, **43**, 5415.
2 M. L. Barsoum, K. M. Fahy, W. Morris, V. P. Dravid, B. Hernandez and O. K. Farha, *ACS Nano*, 2025, **19**, 13.
3 H. Furukawa, K. E. Cordova, M. O'Keeffe and O. M. Yaghi, *Science*, 2013, **341**, 1230444.
4 V. Pascanu, G. G. Miera, A. K. Inge and B. Martín-Matute, *J. Am. Chem. Soc.*, 2019, **141**, 7223.
5 C. J. Doonan and C. J. Sumby, *CrystEngComm*, 2017, **19**, 4044.
6 A. Bavykina, N. Kolobov, I. S. Khan, J. A. Bau, A. Ramirez and J. Gascon, *Chem. Rev.*, 2020, **120**, 8468.
7 Y.-M. Wang, G.-H. Ning and D. Li, *Chem. Eur. J.*, 2024, **30**, e202400360.
8 W.-Y. Gao, A. D. Cardenal, C.-H. Wang and D. C. Powers, *Chem. Eur. J.*, 2019, **25**, 3465.
9 D. Markad and S. K. Mandal, *ACS Catal.*, 2019, **9**, 3165.
10 X. Zhang, L. Chang, Z. Yang, Y. Shi, C. Long, J. Han, B. Zhang, X. Qiu, G. Li and Z. Tang, *Nano Res.*, 2019, **12**, 437.
11 A. Dhakshinamoorthy, N. Heidenreich, D. Lenzen and N. Stock, *CrystEngComm*, 2017, **19**, 4187.
12 D. J. Xiao, J. Oktawiec, P. J. Milner and J. R. Long, *J. Am. Chem. Soc.*, 2016, **138**, 14371.
13 S. Kim, H.-E. Lee, J.-M. Suh, M. H. Lim and M. Kim, *Inorg. Chem.*, 2020, **59**, 17573.
14 A. Phan, A. U. Czaja, F. Gándara, C. B. Knobler and O. M. Yaghi, *Inorg. Chem.*, 2011, **50**, 7388.
15 M. A. Gotthardt, A. Beilmann, R. Schoch, J. Engelke and W. Kleist, *RSC Adv.*, 2013, **3**, 10676.
16 M. Fujita, Y. J. Kwon, S. Washizu and K. Ogura, *J. Am. Chem. Soc.*, 1994, **116**, 1151.
17 W.-Y. Gao, Y. Chen, Y. Niu, K. Williams, L. Cash, P. J. Perez, L. Wojtas, J. Cai, Y.-S. Chen and S. Ma, *Angew. Chem. Int. Ed.*, 2014, **53**, 2615.
18 H. He, Q. Sun, W. Gao, J. A. Perman, F. Sun, G. Zhu, B. Aguila, K. Forrest, B. Space and S. Ma, *Angew. Chem. Int. Ed.*, 2018, **57**, 4657.
19 J. Song, Z. Zhang, S. Hu, T. Wu, T. Jiang and B. Han, *Green Chem.*, 2009, **11**, 1031.
20 C. M. Miralda, E. E. Macias, M. Zhu, P. Ratnasamy and M. A. Carreon, *ACS Catal.*, 2011, **2**, 180.
21 D. Feng, W.-C. Chung, Z. Wei, Z.-Y. Gu, H.-L. Jiang, Y.-P. Chen, D. J. Darensbourg and H.-C. Zhou, *J. Am. Chem. Soc.*, 2013, **135**, 17105.
22 C. Xia, J. Wu, S. A. Delbari, A. S. Namini, Y. Yuan, Q. Van Le, D. Kim, R. S. Varma, A. T-Raissi, H. W. Jang and M. Shokouhimehr, *Mol. Catal.*, 2023, **546**, 113217.
23 T. A. Goetjen, J. Liu, Y. Wu, J. Sui, X. Zhang, J. T. Hupp and O. K. Farha, *Chem. Commun.*, 2020, **56**, 10409.
24 C.-L. Zhang, T. Zhou, Y.-Q. Li, X. Lu, Y.-B. Guan, Y.-C. Cao and G.-P. Cao, *Small*, 2023, **19**, 2205898.
25 T. A. Goetjen, J. G. Knapp, Z. H. Syed, R. A. Hackler, X. Zhang, M. Delferro, J. T. Hupp and O. K. Farha, *Catal. Sci. Technol.*, 2022, **12**, 1619.
26 B. Liu, S. Jie, Z. Bu and B.-G. Li, *J. Mol. Catal. A Chem.*, 2014, **387**, 63.
27 R. J. Comito, K. J. Fritzsching, B. J. Sundell, K. Schmidt-Rohr and M. Dincă, *J. Am. Chem. Soc.*, 2016, **138**, 10232.
28 R. J. Comito, Z. Wu, G. Zhang, J. A. Lawrence III, M. D. Korzyński, J. A. Kehl, J. T. Miller and M. Dincă, *Angew. Chem. Int. Ed.*, 2018, **57**, 8135.
29 R. J.-C. Dubey, R. J. Comito, Z. Wu, G. Zhang, A. J. Rieth, C. H. Hendon, J. T. Miller and M. Dincă, *J. Am. Chem. Soc.*, 2017, **139**, 12664.
30 I. Rodrigues, I. Mihalcea, C. Volkringer, T. Loiseau and M. Visseaux, *Inorg. Chem.*, 2012, **51**, 483.
31 Q. Fu, H. Ranji-Burachaloo, M. Liu, T. G. McKenzie, S. Tan, A. Reyhani, M. D. Nothling, D. E. Dunstan and G. G. Qiao, *Polym. Chem.*, 2018, **9**, 4448.
32 H. L. Nguyen, F. Gándara, H. Furukawa, T. L. Doan, K. E. Cordova and O. M. Yaghi, *J. Am. Chem. Soc.*, 2016, **138**, 4330.
33 Y. Liu, D. Chen, X. Li, Z. Yu, Q. Xia, D. Liang and H. Xing, *Green Chem.*, 2016, **18**, 1475.
34 H.-C. Lee, M. Fantin, M. Antonietti, K. Matyjaszewski and B. V. K. J. Schmidt, *Chem. Mater.*, 2017, **29**, 9445.
35 C. J. Chuck, M. G. Davidson, M. D. Jones, G. Kociok-Köhn, M. D. Lunn and S. Wu, *Inorg. Chem.*, 2006, **45**, 6595.
36 Z. Luo, S. Chaemchuen, K. Zhou, A. A. Gonzalez and F. Verpoort, *Appl. Catal. A Gen.*, 2017, **546**, 15.
37 P. Mialane, C. Mellot-Draznieks, P. Gairola, M. Duguet, Y. Benseghir, O. Oms and A. Dolbecq, *Chem. Soc. Rev.*, 2021, **50**, 6152.
38 H. M. Tran, L.-T. T. Nguyen, T. H. Nguyen, H. L. Nguyen, N. T. S. Phan, G. Zhang, T. Yokozawa, H. L. Tran, P. T. Mai and H. T. Nguyen, *Eur. Polym. J.*, 2019, **116**, 190.
39 C. Hu, X. Wang, Y. Lan, L. Xiao, S. Tang and L. Hou, *Eur. Polym. J.*, 2024, **203**, 112695.
40 C.-Y. Tsai, F.-Y. Cheng, K.-Y. Lu, J.-T. Wu, B.-H. Huang, W.-A. Chen, C.-C. Lin and B.-T. Ko, *Inorg. Chem.*, 2016, **55**, 7843.
41 T. Islamoglu, K.-i. Otake, P. Li, C. T. Buru, A. W. Peters, I. Akpinar, S. J. Garibay and O. K. Farha, *CrystEngComm*, 2018, **20**, 5913.
42 Z. H. Syed, M. R. Mian, R. Patel, H. Xie, Z. Pengmei, Z. Chen, F. A. Son, T. A. Goetjen, A. Chapovetsky, K. M. Fahy, F. Sha, X. Wang, S. Alayoglu, D. M. Kaphan, K. W. Chapman, M. Neurock, L. Gagliardi, M. Delferro and O. K. Farha, *J. Am. Chem. Soc.*, 2022, **144**, 16883.
43 T. E. Webber, S. P. Desai, R. L. Combs, S. Bingham, C. C. Lu and R. L. Penn, *Cryst. Growth Des.*, 2020, **20**, 2965.

The data supporting this article have been included as part of the Supplementary Information.